Eleventh International Conference on Computational Fluid Dynamics (ICCFD11), Maui, Hawaii, July 11-15, 2022

ICCFD11-2022-4004

Validation of the new modeling capabilities of the Ansys Fluent CFD high-speed solver for the simulation of supersonic combustion in Scramjets and Rotating Detonation Engines

B. Crawford, I. Verma, S. Orsino, J. Cagnone, and S. Li*,**
Corresponding author: bruce.crawford@ansys.com
Ansys, Inc, Canonsburg, PA, 15317, USA

Abstract: With the rise in interest in new hypersonic propulsion systems in the past few years, there has been a push to improve the predictive capabilities of numerical tools such as CFD; these tools provide unmatched capabilities for the design and analysis of such propulsion systems. In the present work we focus on the recently expanded capabilities of the Ansys Fluent CFD high-speed Density Based Navier-Stokes (DBNS) solver to improve i) the solver speed and ii) the fidelity for the modeling and design of supersonic combustion ramjet engines (Scramjets) and rotating detonation engines (RDE).
The summary of the work being presented here will show the validation of the new capabilities of Ansys Fluent CFD. The DLR, Burrows-Kurkov Scramjet, and AFRL/NETL RDE experiment tests and model geometries are used for the CFD modeling and results validation. DLR scramjet and AFRL RDE geometries are meshed using Ansys Fluent Poly-Hexcore Mosaic meshing, in which these meshes are used to assess the global combustion model with the direct source method solution speed capabilities and using detail chemistry kinetic mechanism. The validation cases presented use the spectrum of turbulence models for the validation, with the Realizable KE, K-Omega SST, and LES.

Keywords: Computational Fluid Dynamics, Turbulence Modeling, Combustion Modeling, Density Based Solver.

1 Introduction

The design of air breathing propulsion systems for high-speed vehicles presents several challenges to the aerospace community. The challenges range from the difficulty in understanding the fundamental high-speed reacting flow physics to the development of a reliable system design that can work for the different flight conditions of the mission.

Designers have several tools at their disposal to analyze and understand high-speed reacting flows, including physical testing, theoretical analysis, and numerical simulations. However, given the high speed and extremely high temperatures involved, experimentation and theory are limited in what they can accurately measure and predict. For example, notwithstanding the excessive costs of operating a high-speed reacting wind tunnel, it is virtually impossible for a ground-based facility to match all the important flight conditions; in addition to that, these facilities can only create relatively short run-times [1].

At the other end of the spectrum, theoretical analysis has provided extremely useful insights, but it is hindered by the class of problems and geometric complexity it can properly handle since the governing equations are highly non-linear and the gas cannot be treated as calorically perfect, thus making impossible a closed-form solution. Numerical simulations represent a viable method to study hypersonic flows that sits in between experimentation and theory. Computer simulations can reproduce virtually any flight condition, and the continuous solution field can be probed at any location to extract any parameters of interest. However, care must be taken in setting up properly the simulation since the combination of complex flow physics and the “stiff” behavior of the numerical schemes can create its own challenges; lack of convergence, convergence to the wrong solution, mesh dependency and incorrect physics [2]-[4]. The vast majority of the previous simulation work with Scramjets [12]-[17] and RDEs [21]-[23] combustor have employed pressure-based CFD solvers. Conversely, the current simulations are performed using a density-based solver. More specifically, we focus on the Ansys Fluent density-base solver (DBNS) with two families of air-breathing high-speed propulsion systems: the supersonic combustion ramjet (scramjet) engines [5] and rotating detonation engines (RDE). Both types of engines present distinct advantages and some challenges. The cases chosen for the validation effort are two Scramjet cases, the Burrows-Kurkow [7] and the DRL setup [10] and one for the RDE, the AFRL/NETL case [20].

2 Test Cases

Below is a detailed description of the three cases selected for the solver testing and validation study. The operating conditions for the study of the four cases are summarized in Table 1. The AFRL/NETL RDE is run for two different model and mesh settings.

	Burrows-Kurkov		**DLR**		**AFRL/NETL RDE**	
	Air	Fuel	Air	Fuel	Air	Fuel
Mach Number	2.44	1.0	2.0	1.0	na	na
U(m/s)			730	1200	na	na
T_o (K)	1270	254	340	250	300	300
T_W (K)	298		Adiabatic		Adiabatic	
P_o (kPa)	101.352	101.352	101.325	101.325	350.000	450.000
MassFlow (kg/s)	-	-	-	-	0.63	0.018
Fuel	Hydrogen		Hydrogen		Hydrogen	
Y_{O2}	0.258	0.0	0.232	0.0	0.2333	-
Yn_2	0.486	0.0	0.736	0.0	0.7667	-
Y_{h2o}	0.256	0.0	0.032	0.0	-	-
Y_{h2}	0.0	1.0	0.0	1.0	-	1.0
Solver Time	Steady State		Steady State		Transient	
Turbulence model	SST K-Omega		SST K-Omega		RKE EWF	SST K-Omega
CFD geometry: 2D/3D	2D-planar		3D-single injection passage		3D	
CFD Mesh type	Hexahedral		Poly Hexcore		Poly Hexcore	
Number Cells	34853		1104239		1408939	2848292

Table 1: Operating conditions and model settings for the validation cases.

2.1 Burrow-Kurkov Supersonic Combustion

The first case being evaluated is based on the supersonic combustion experiments performed by Burrows and Kurkov [7] as well as CFD simulations of Engblom et al. [8] and Vyas et al. [9]. The test geometry is shown Figure 1(a) and the test condition are summarized in Table 1. The flow conditions being used are same used by Vyas et al. [9] in their numerical simulation. The present simulation focuses on a finite-rate, hydrogen-air chemical mechanism also used by Vyas et al. in a Mach 2.44 flow with vitiated air. The analysis investigates the ignition point and the species mole fraction of the combustion products. Four different combustion solvers available in Ansys Fluent are assessed: the React to Equilibrium, Direct Source, Stiff Chemistry (ODE), and the TCI EDC PaSR models from Ferrarotti et al. [19]. The 9-species and 18-reaction kinetic mechanism from [9] was used with the default settings for each combustion solver. The flow and species transport-equations are solved monolithically, using the Fluent Density-Based Navier Stokes (DBNS) coupled solver [24] [25].

Using Ansys SpaceClaim Meshing [24], a 2D structured grid of size 34853 was created comparable to the Vyas et al. [9] as shown in Figure 1(b). The wall boundaries are no-slip condition with fixed temperature of 298 K.

.

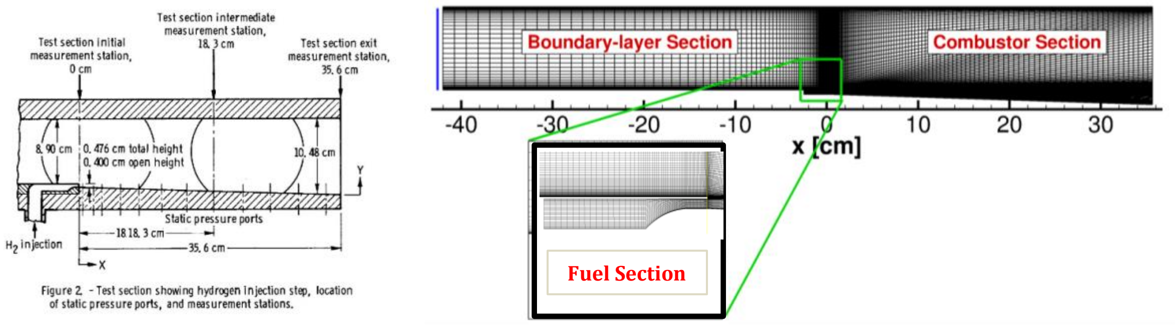

(a) (b)

Figure 2. Burrows and Kurkov supersonic slot combustor (a) Geometry [1] and (b) mesh [2].

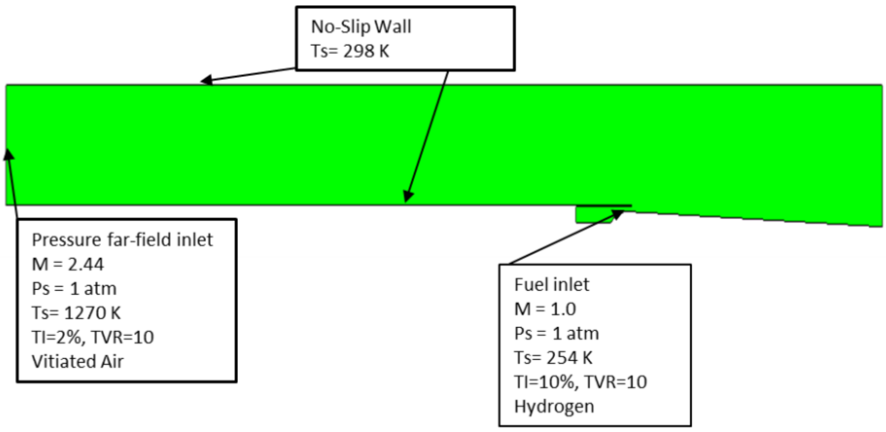

Figure 2: Boundary conditions of the 2D Borrow-Kurkov supersonic combustor.

2.2 DLR Scramjet Model

The second case under consideration is the DLR supersonic combustor experiment by Waidmann et al. [10] shown in figure 3(a). This is a strut injection configuration with multiple holes. For this current evaluation we are running this 3D with one injector for Steady state cases. Ansys SpaceClaim was used to create the geometry described in [10] [12] [13] and shown in Figure 3(b). Other researchers have modeled the DLR with different CFD solvers and different methods [12]-[16]. In the present work we are using the same conditions test conditions and we are resolving one fuel injection and shown in Figure 4(b). The flow conditions being used are for a Mach 2.0 vitiated main flow with a Mach 1.0 inject for fuel stream at atmospheric pressures, also presented in Table 1. The analysis investigates the flame mixing and the species mole fraction of the combustion products. As with the Burrow-Kurkov combustion case, we are evaluating the performance of four different combustion solvers available in Ansys Fluent: The React to Equilibrium, Direct Source, Stiff Chemistry (ODE), and the TCI EDC PaSR models from Ferrarotti et al. [19]. The Li et al. [18] hydrogen/air reaction kinetic mechanism that has 9 species/ 21 was used with the default settings for each combustion solver being evaluated using Fluent Density Base Navier Stokes (DBNS) coupled solver [24] [25].

The DLR model was meshed using Ansys Fluent Meshing [24] and the final mesh is shown in Figure 4., the mesh shown in this picture is fully 3D with poly-hexcore cell topology with minimum core cell size of 0.4mm and with a 0.1mm mesh refinement area around the fuel injector. A boundary layer mesh with 12 layers is used around the strut and test section walls, with fixed boundary layer first high of 0.02mm. The total number of cells is 1,104,239. All the walls are assumed to be adiabatic with a no-slip condition and pressure-far field boundaries with the condition shown in Table 1.

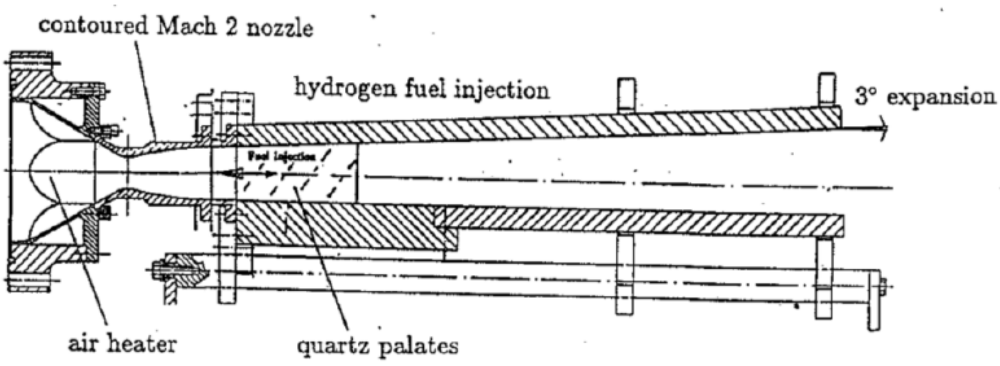

(a)

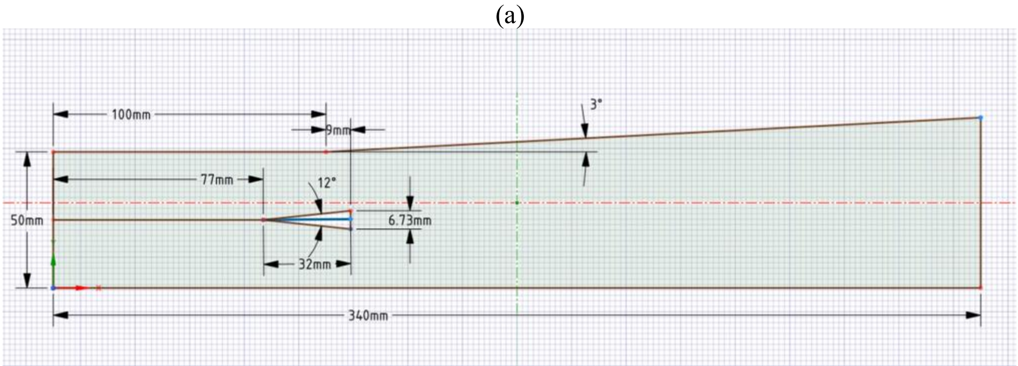

(b)

Figure 3: DLR Scramjet Geometry (a) and computational domain (b) used in the present study.

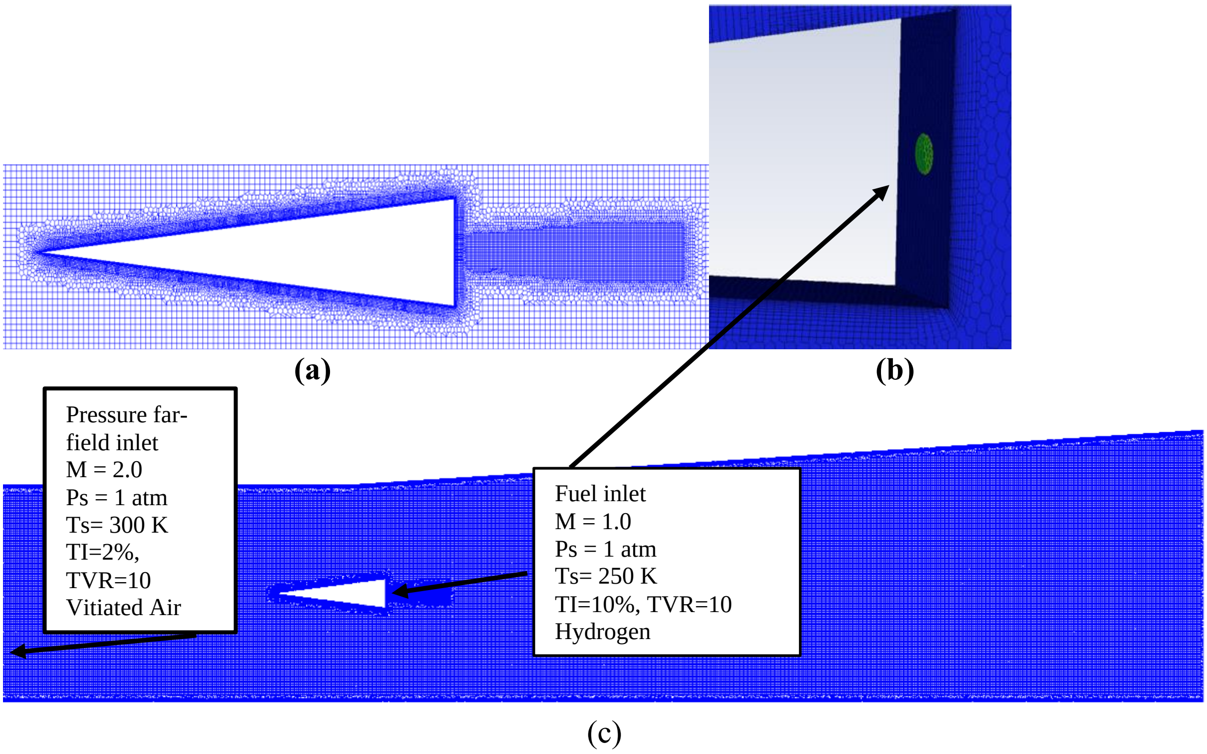

Figure 4: Computational grid 3D Poly-Hexcore; (a) base mesh and inlet boundary conditions, (b) fuel injector inlet mesh and base mesh, (c) section plane of the injector stream refinement and strut shear layer refinement meshes. Base mesh is 0.4mm with refinement area of 0.1mm.

2.3 AFRL/NETL RDE

This RDE case is based on the test done by AFRL, Rankin et al. [20] for hydrogen/air RDE tests shown in Figure 5(a). Presented are two cases that represent distinct levels of fidelity of modeling the supersonic combustion: Case 1, performance predicting model, fast solving, and Case 2 modeling detailed chemistry and boundary layer mesh resolution. Case 1 which has the coarse mesh, Realizable KE model with Enhance wall function was used for turbulence closure. With Case 2, the turbulence will be modeled using the K-Omega SST with only the compressibility effects as the only options for both cases.

Two different models were used in the RDE cases for ignition and deflagration to detonation reaction chemistry. A tune one-step hydrogen reaction Strakey et al. [21] and was solved with the Direct Source Method solver for Case 1 simulation. Case 2 mesh, the Li et al. [18] hydrogen/air reaction kinetic mechanism that has 9 species and 21 reactions was used Stiff Chemistry solver [24] [25] with direct integration and the default settings. Each case was initialized by fuel and air mixture from a steady state solution into the combustion section (Figure 7), using the flow conditions summarized in Table 1. Both solutions are ignited from a pulse detonation tube section, providing the pressure/temperature shock pulse required to start the RDE to reach detonation flame in the combustion section. For both cases, a time-step 3.5×10^{-7} seconds was used for the simulation, which equated to approximate 720 time-steps per period of the detonation wave.

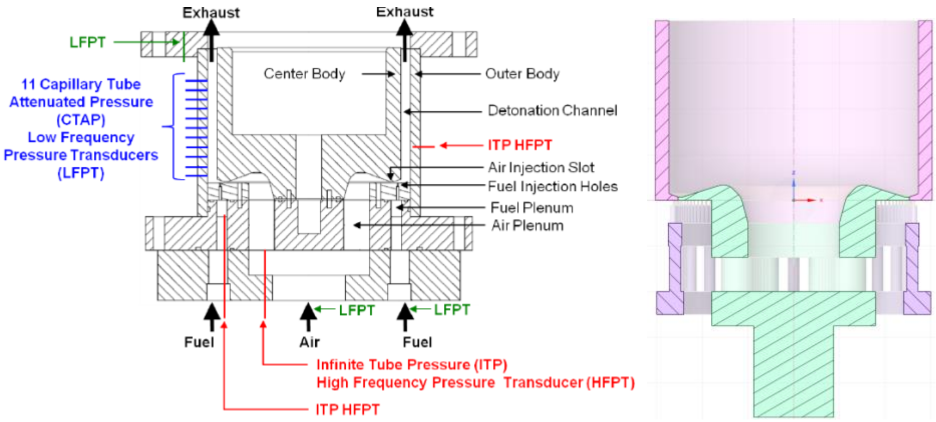

(a) (b)

Figure 5: AFRL/NETL RDE (18) geometry diagram(a) and the Ansys Space Claim geometry (b) created for use in the mesh creation for the different cases being evaluated.

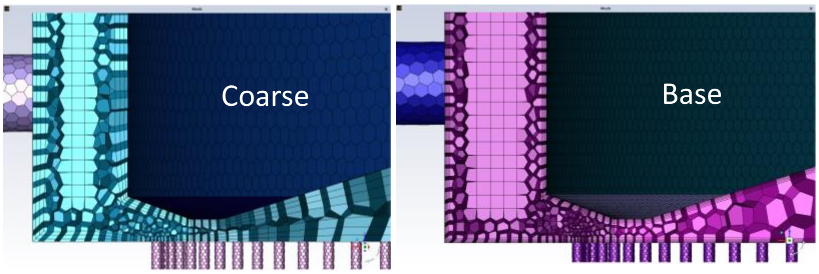

Figure 6: The different case meshes being used for model validation: (a) Coarse mesh for performance modeling; (b) Base mesh for chemistry and future thermal modeling; All are Poly-Hexcore mesh from Ansys Fluent Meshing. Please refer to Table 1. For mesh stats.

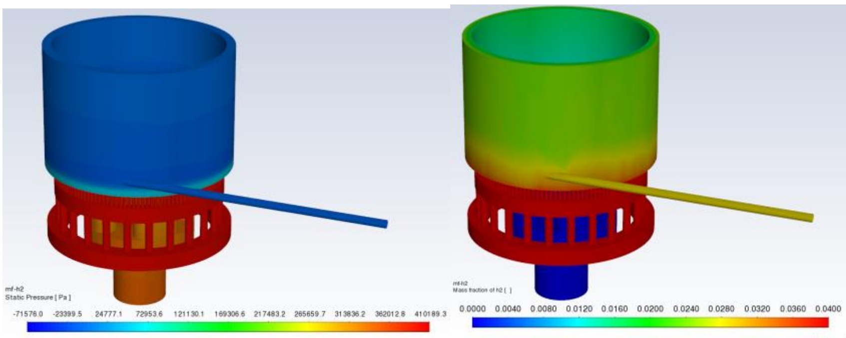

Figure 7: Steady State Initial Condition setup (a) Pressure contour and (b) hydrogen mass-fraction contour and RDE ignition process.

The AFRL/NETL geometry shown in Figure 5(a) was provided by Peter Strakey [21] and was used to create a geometry in Ansys SpaceClaim. The RDE model was meshed with Ansys Fluent Meshing creating a 3D mesh using the poly-hexcore topology. The combustor mesh for the performance case a cell size of 1.5mm was used and 3 layers of boundary layer mesh using the smooth transition offset method provided a mesh size of 1,408,939 cells shown in Figure 6(a). Figure 6(b) shows the base mesh case with a 1.0mm size combustor mesh and 5-layer boundary layer mesh using uniform offset method with first cell height of 0.05mm creating a mesh size of 2,848,292 cells. All the wall boundaries are assumed adiabatic and with a no-slip condition. The flow boundaries are mass-flow inlet boundaries and pressure outlet boundary with the condition shown in Table 1.

3 Numerical Approach

3.1 Flow Solver

All the numerical simulations in the present work were run using the commercial CFD code Ansys Fluent [24] [25]. Fluent is a widely used cell-centered finite-volume code that solves the Reynolds-Averaged Navier-Stokes (RANS) equations. The Fluent solver offers the option to solve the RANS using either a pressure-based implicit solver (PBNS) [26] [27] or a density-based implicit or explicit solver (DBNS) [28] [29], either in steady-state or unsteady mode.

The four simulations presented here were performed using the Fluent DBNS solver. The Roe Flux-Difference Splitting formulation were used for the calculation of the convective fluxes. A second-order upwind spatial discretization is achieved using the Least-Square (LSQ) cell-based gradient formulation. Barth and Jespersen [30] gradient-limiter is utilized to prevent spurious oscillation of the flow solution near shocks and flow discontinuities. The viscous fluxes are computed from the average of unlimited-reconstruction of field variables on the control volume faces. This is equivalent to a second-order central-differencing scheme. For unsteady simulation, the solution is advanced in time using a second-order Backward-Euler implicit temporal discretization. The system of equations is solved using the Incomplete Lower Upper (ILU) decomposition smoother in conjunction with a coupled Algebraic Multigrid Method (AMG) solver. Also used is Fluent DBNS solver adaptive High-Speed Numerics option [24] [25]. Adaptive "High-speed Numerics" is used to help in stabilizing and accelerating the convergence for high-speed flows for steady-state solutions by adjusting the numerics proportionally to the strength of the captured shockwave.

Two different closure models are used in these cases to model turbulence quantities, the default K-Omega SST model was used for the steady state scramjet cases. For the base case RDE models, the one-step chemistry coarse mesh case the Realizable K-E turbulence model with the Enhanced Wall Function [EWF] [24] [25]. The default settings and constants were used for each model with the compressible effects only option selected.

3.2 Chemistry Solvers

All cases used finite rate chemistry for the modeling of the high-speed reacting flow in the model. With the steady state cases, the choices of solvers used are the Relax to Equilibrium (RTE), Direct Source Method (DSM) and Stiff Chemistry solver (ODE methods) [24] [25]. DSM treats the finite-rate reactions as source-term to the species equation, along with their exact linearization, thus maximizing the robustness and iterative convergence of DBNS' strongly coupled implicit solution method. The Relax to Equilibrium solver is good approximation with no reaction and was used to initialize the solution that need to be artificially ignited to start reaction. These are all setup to work with no-TCI, the TCI method being used is from Ferrarotti et al. [19] based on dynamic Partially Stirred Reactor (PaSR).

Finite rate with DSM and Stiff Chemistry models with no-TCI [24] [25] were utilized for the transient RDE cases for modeling the ignition and detonation combustion processes.

3.3 Meshing and Boundaries

Ansys Fluent is capable of handling both structured and unstructured (Tetrahedral, Cut-cell, Polyhedral, Poly-Hexcore, etc.) mesh topologies. In the present study, the meshes were generated using two approaches for the 2D meshes, the Ansys SpaceClaim Meshing tool was used. The 2D mesh contains only quadrilateral elements since the geometries under consideration are simple and a hexahedral mesh was readily applied to the domain using automatic domain decomposition. For the 3D meshes, the Water-Tight method (WTM) workflow within the Ansys Fluent Meshing tool was employed. Unstructured poly-hexcore meshes were develop for both the DLR geometry and the RDE geometry models. For the turbulent cases, the unstructured meshes were developed to ensure a y+~1.0 on all the wall surfaces, except for the RDE using RKE turbulence model case.

Because of the density variations, sonic, and supersonic conditions at the inflow and fuel injectors in the scramjet simulation, the Pressure Far-Field boundary and the Static Pressure were selected for the inlets and outlet boundaries. A new “Flux-Based” Pressure Far-field option was employed for these inlet flows, which is more robust and accurate and improves convergence for these types of solution compared to the default Riemann invariant method available. Mass-flow inlets and Static Pressure outlet boundaries were utilized for the RDE transient cases.

4 Results

4.1 Burrows-Kurkov supersonic combustor results

The first validation study is of the Burrows-Kurkov supersonic combustor experiment [7], which is a surface injection of hydrogen fuel from the slot into a diverging combustor. The test flow conditions are sufficient for autoignition, but to reduce solver time each simulation case was initialized from the FMG initialization solution using the RTE chemistry solver. From this initialization several runs with the four distinct combustion solvers were performed using the DBNS solver [24] [25]. Figure 8 shows the results of the temperature contours showing the flame locations in the combustor for each mode. The experiment shows the flame approximately at 11.0cm. Comparing the four solutions, RTE and Stiff Chemistry (ODE) show the flame at the 8-9cm. Whereas the DSM Figure 8(b) and EDC PaSRd solutions show the flame position at 12.0cm and 21cm. Comparing the models, the flame strength is different for each solvers, but the PaSRd model is the closest to the test. The PBNS steady-state solver could be contributing to differences in the with the convergence on the sources for each chemistry solver. And with using default turbulence settings could be affecting the solution predictions also, change diffusion mixing and species transport.

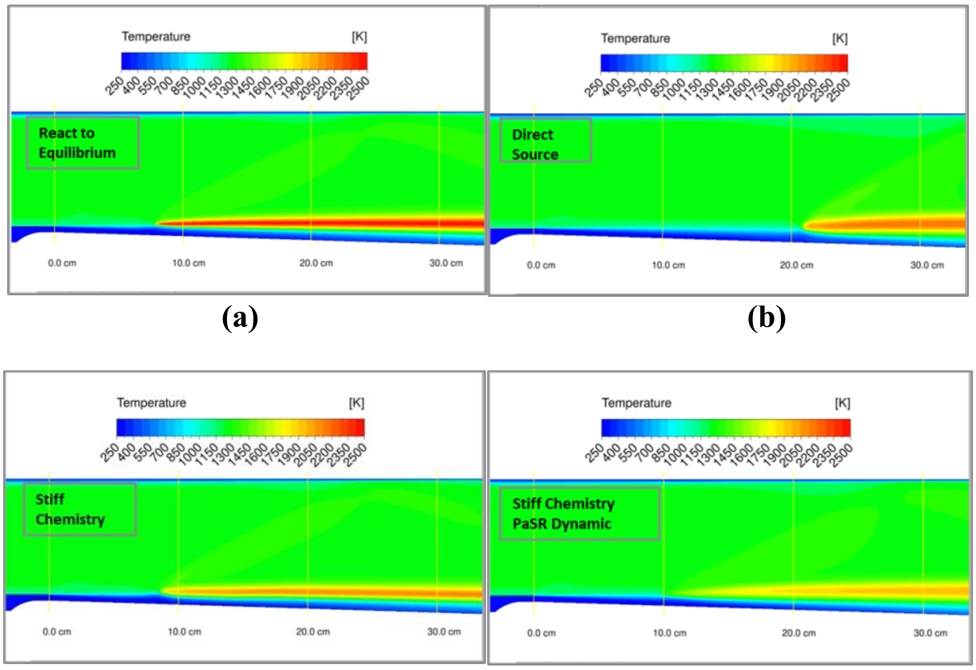

(a) (b) (c) (d)

Figure 8: Flame location for each model solution: (a) React to Equilibrium (b) Direct Source Method (c) Stiff Chemistry and (d) EDC PaSR Dynamic

When we compare the total temperature profiles to the Burrows-Kurkov test [7], we see a different trend at the outlet of the models shown in Figure 9. The RTE model shows the peak total temperature with the test, and PaSRd solution under predicts the peak total temperature. The DSM profile agrees the best with the test data. Whereas the Stiff Chemistry solution does not burn as fast or as long as the others, but the peak is similar magnitude to the DSM solution which is expected.

The opposite is seen in solutions when we compare the Mach number outlet profiles to the test. The Stiff Chemistry solution shows good agreement with the Mach number profile shown in Figure 10. While the Direct Source method shows an over and then under prediction of the Mach number along the outlet profile, the RTE shows the best agreement in the first part of the profile and at the end of the profile looking at the test Mach number. The PaSRd solution looks like a mean between all the solution and test results. The heat release from the flame with Stiff Chem solver is much less than the other models in the total temperature profile. The Direct Source method does show more heat release to the flow and has the most effect on the Mach number profile, slowing down the flow. Key take away from each solution, is that the combustion solvers are working with the DBNS solver and providing comparable solutions to the test results with defaults. The turbulence model options and combustion settings could account for these differences between data and solutions and need to be further investigated in future simulations. The assessment of the EDC PaSRd model shows the need of improvements to work with these high-speed reacting flows.

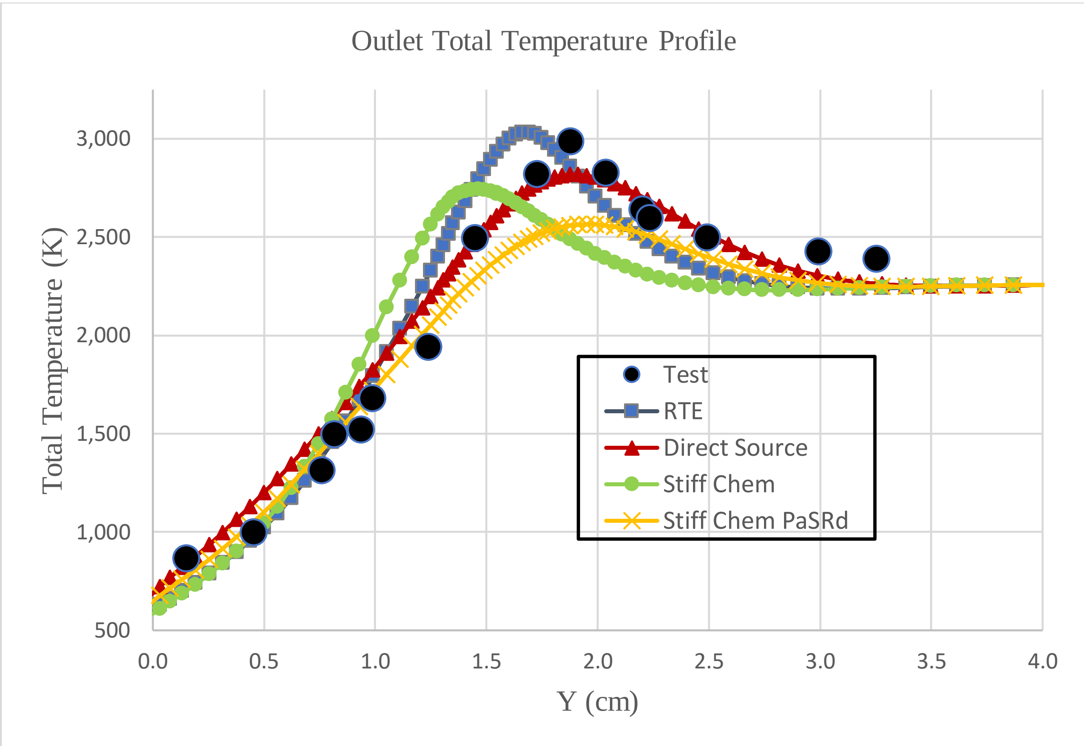

Figure 9: Total temperature results at outlet of the Burrows/Kurkov supersonic combustor, comparing different combustion models to the test results

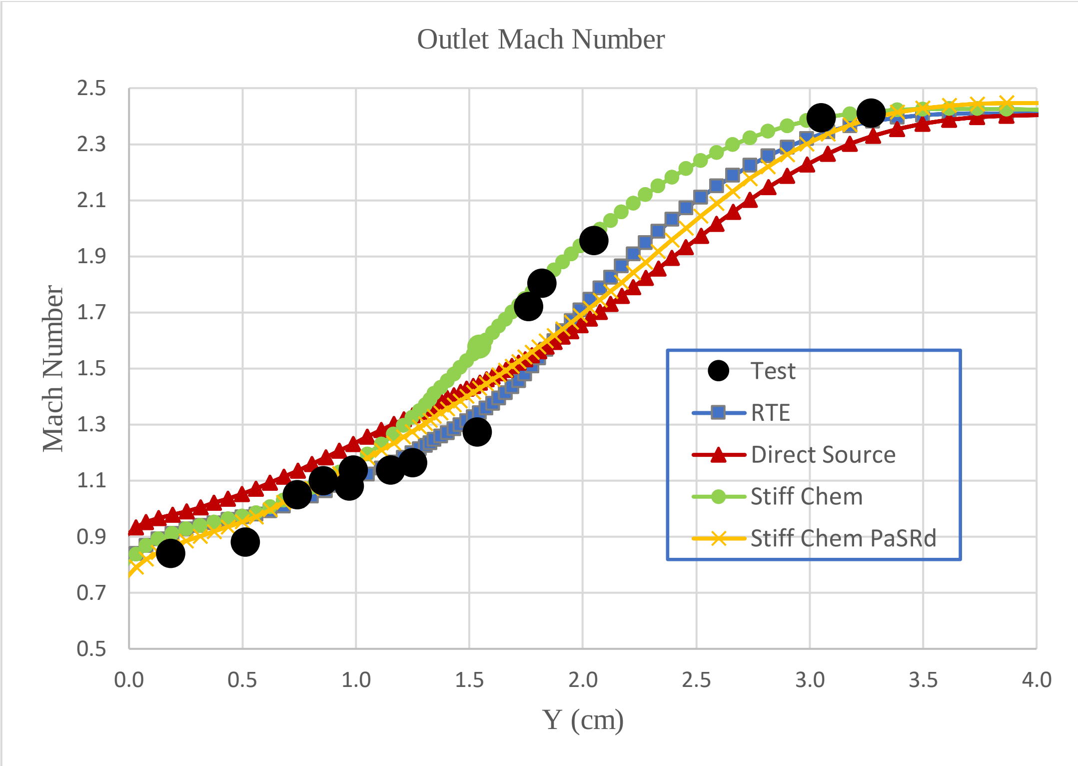

Figure 10: Mach number results at the outlet of the Burrows/Kurkov supersonic combustor, comparing different combustion models to the test results

4.1 DLR Scramjet

The next validation case is the DLR strut combustor experiment performed by Waidmann et al. [10], which is a test of a supersonic combustor injector strut testing the fuel air mixing and flame stability. The experimental flow conditions are not enough to induce shock ignitions of the flame so as in the experiment, the simulation was ignited via numerical means. This was accomplished by using RTE solver with the FMG initialization process in Fluent solver [24] [25], this solution was used to initialize the DBNS solutions with the other chemistry solver. Figure 11 shows the converge solutions of each case of the static temperature contours at the midplane of the DLR strut combustor. This shows hydrogen flame lift off from the strut for the different chemistry solvers and the effect of the each on the flow behind the strut. Higher temperature flame is seen with Stiff Chem solver showing faster reaction (heat release) in the mixture zones. Each of the other three chemistry solvers show similar flame zones, with DSM solver with widest flame zone and PaSR show the diffuse, lower temperature flame zone.

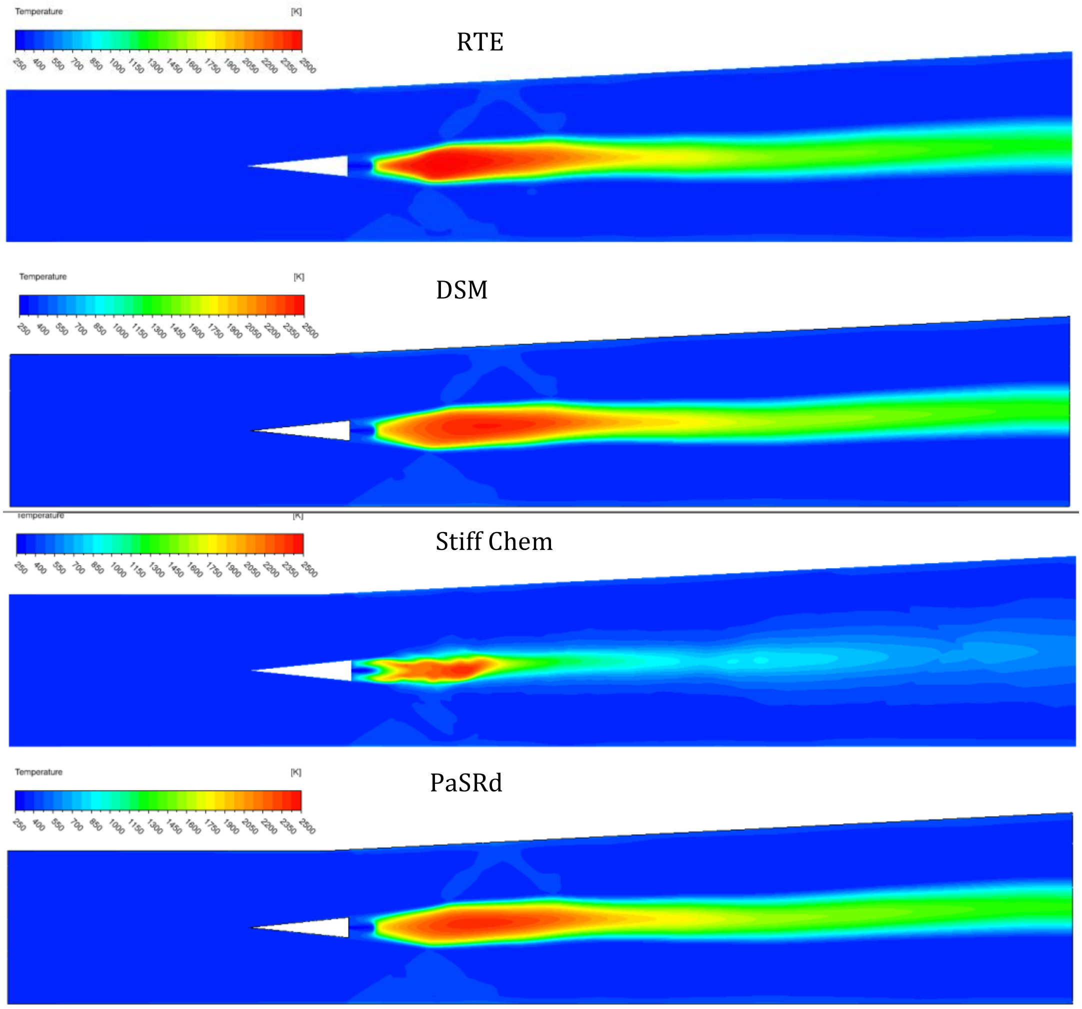

Figure 11: Static Temperature center plane contour results of the DLR combustor, comparing different combustion models

The static pressure midplane contours are shown in Figure 12, each showing the effects the combustion flame on the pressure field. The Stiff Chem case flame zone has minimal effect on the pressure field, were as the RTE and DSM case has the strongest pressure increase, and PaSRd case is slightly less. The density gradient contours in Figure 13 show this in more detail, displaying the effects of each flame zone on the shock train. In comparing RTE and DSM solver density gradient contours, a shift in the shock train can be seen between the two solver solutions, damping the shock train strength in the DSM solution.

Figure 14 compares the results to experiment data from Waidmann et al. [10], which displays the temperature profiles at 120mm down-stream of the main air inlet. The only results that do not agreed with the test results is the Stiff Chemistry solution, where the temperature is significantly higher in the profile. These differences to solutions could be contributed to the mesh size, which in turn would affect the mixing and diffusion of the fuel into the main flow. Additionally, the use of the default settings for the turbulence and combustor models also could be contributing to the differences. The main goal of the exercise was to see the functionality of the new and updated combustion models within the DBNS solver, for which the results showed this was attained. Also, not quantified here were the improvements implemented in DBNS solver's robustness and efficiency. Showing the ability to converge these solutions to a lower residual with 15X less iterations compared to earlier releases of the DBNS solver. As previously mentioned with the Burrows-Kurkov case, future work with the DLR model will be investigated to improved prediction with adjustments to the turbulence and combustion model settings.

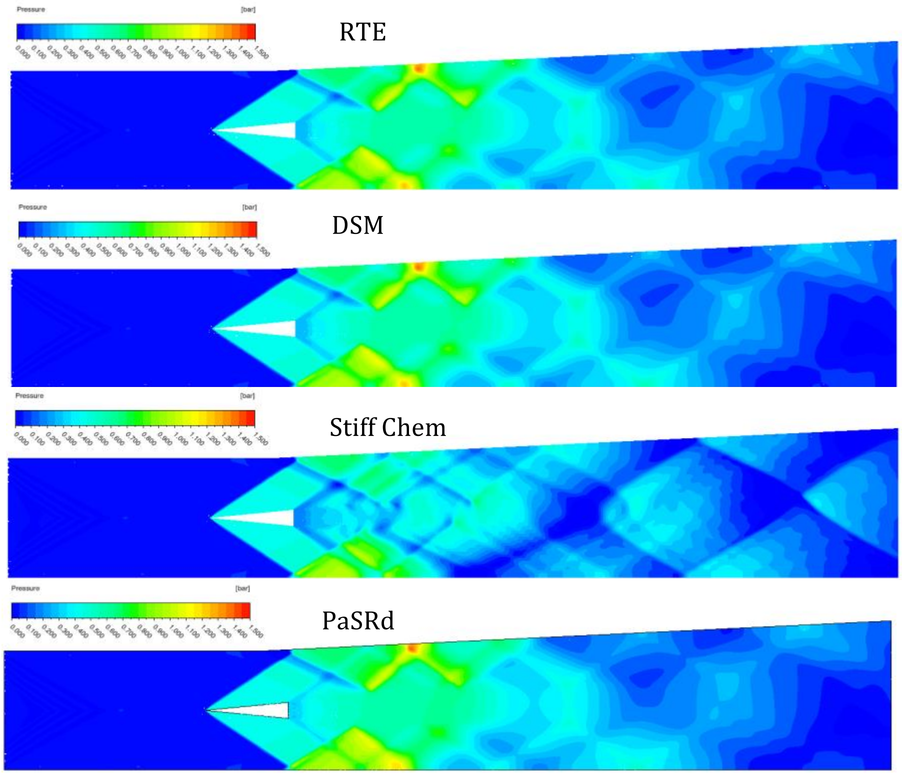

Figure 12: Static Pressure center plane contour results of the DLR combustor, comparing different combustion models.

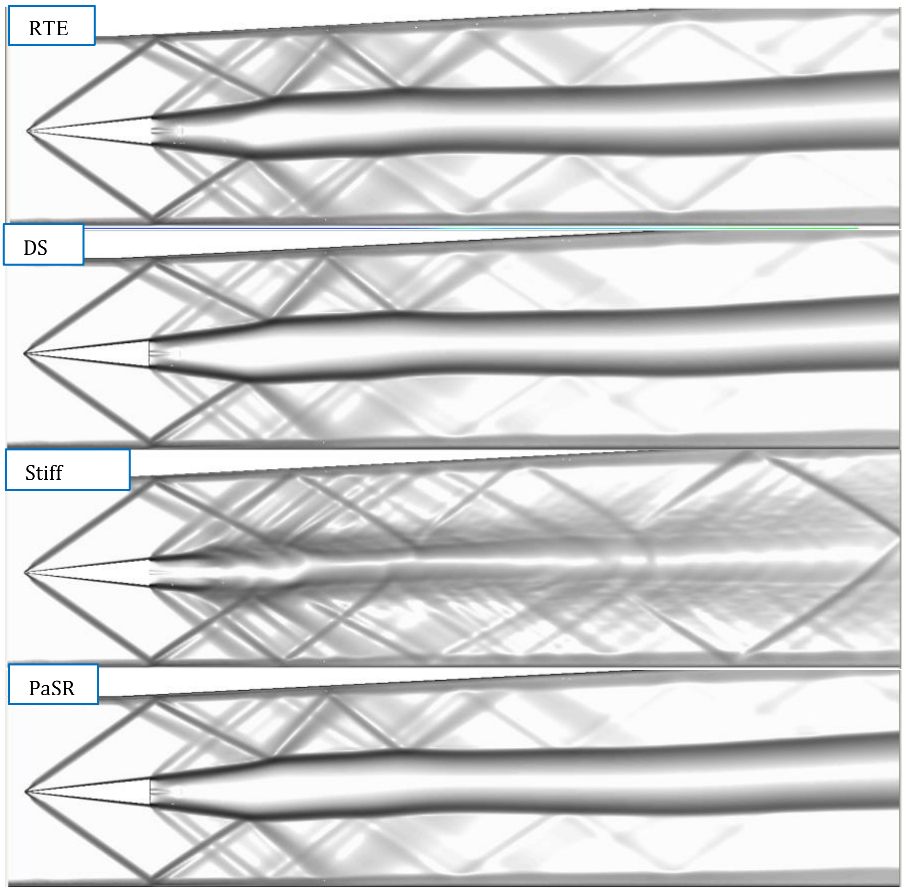

Figure 13: Density Gradients at the center plane, showing shock and flame interaction within the DLR combustor, comparing different combustion models.

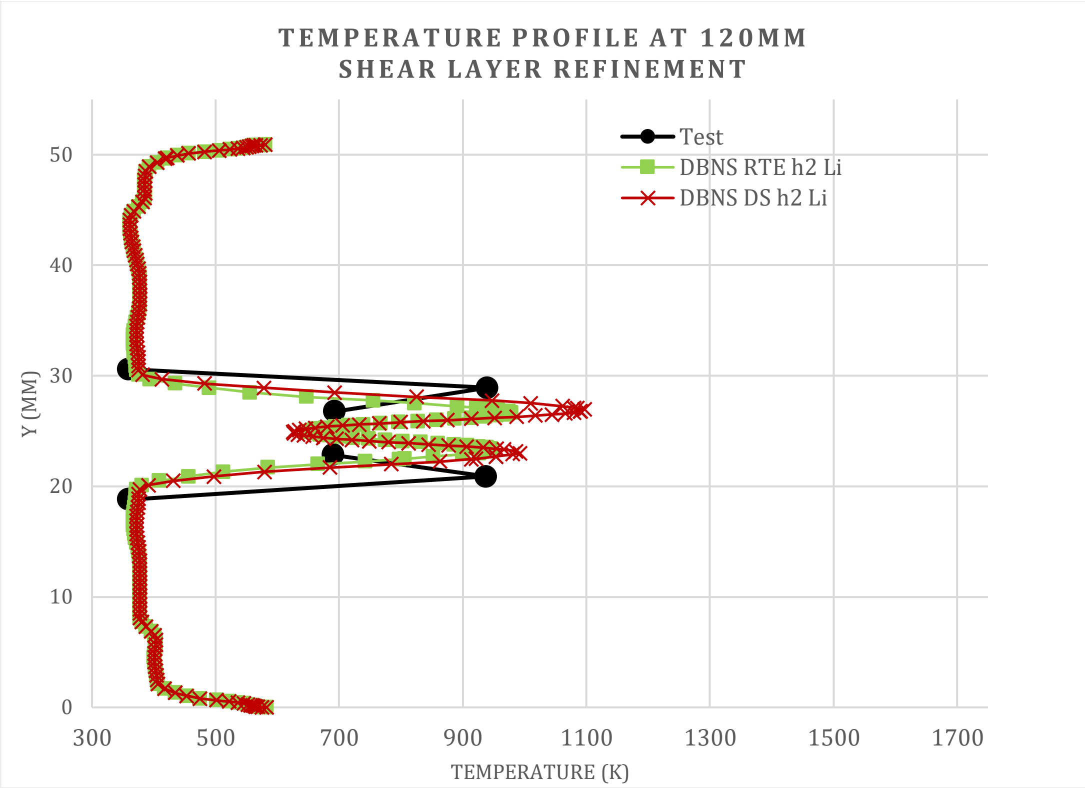

(a)

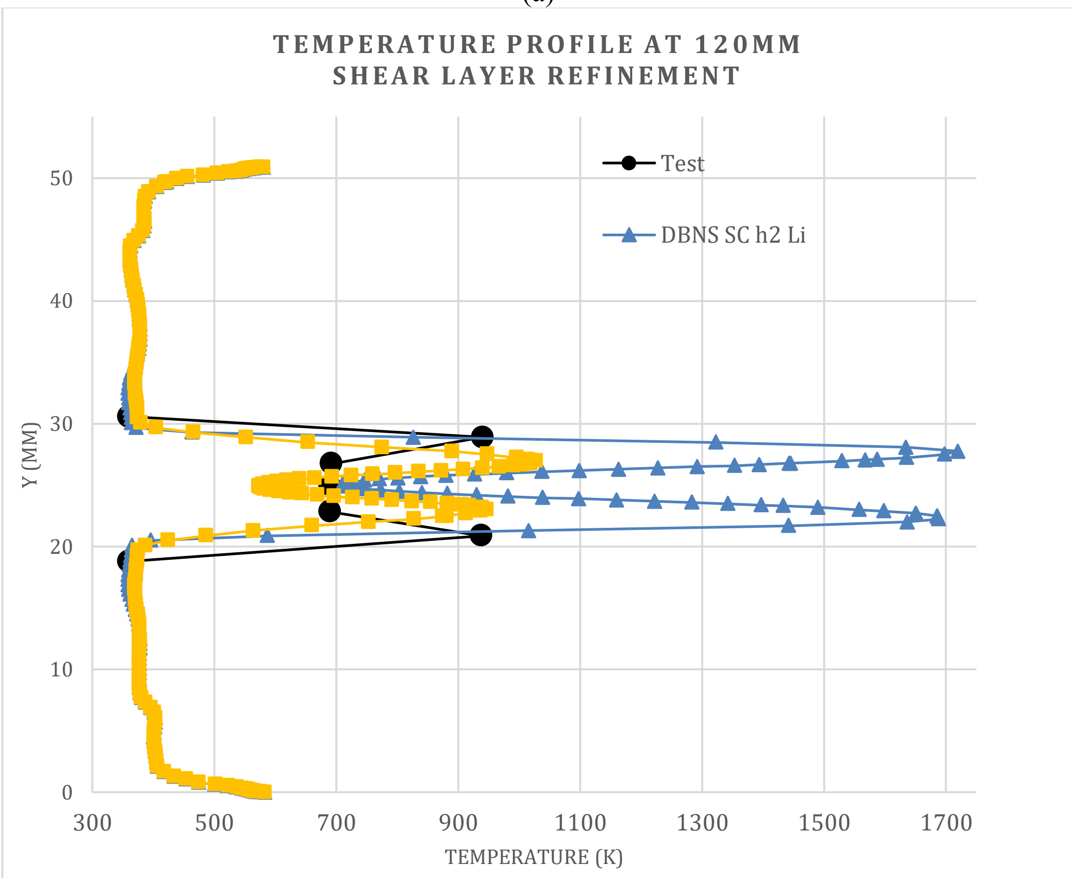

(b)

Figure 14: Static Temperature profile at 120mm location in the DLR combustor. (a) RTE, DSM (b) Stiff Chemistry, PaSRd combustion models comparison to the test results

4.3 AFRL/NETL RDE

The last validation case consists of a hydrogen/air Rotating Detonation Engine (RDE), experimentally studied at the AFRL by Rankin et al. [20]. The propulsive energy of an RDE engine is generated by a supersonic detonation front, which travels along the circumference of a circular apparatus, consuming a mixture of fuel and air injected from below. Figure 15 shows the shockwave predicted by the one-step mechanism and k-epsilon turbulence model. The shock travels in a clockwise motion in the reactor, where the increase in pressure downstream of the shockwave is readily observed. An increase in temperature, caused by the recompression and ignition of the fuel-oxidizer mixture, is also noted. Figure 16 shows the temporal history of pressure probes in the combustion chamber. A periodic solution is observed after 0.0018 seconds, with a wave frequency of about 3.6 kHz. Figures 17 and 18 present a similar comparison, this time using Li's hydrogen mechanism, the k-omega SST turbulence model, and a moderately refined grid. Using this model, the shock wave travels in the counterclockwise direction and the pressure increase across the shockwave is more diffuse. The pressure history shown in Figure 18 confirms that while the wave frequency is similar to the previous case, the pressure peaks are about 40% lower. Looking at the pressure trace data, you can see that the one-step case does not go through the deflagration to detonation process as the Li's hydrogen model case does, showing the solver able to manage this transition process with the settings employed. Finally, Table 2 presents a quantitative comparison of the wave velocities and pressure measurements with previous experimental and numerical results [1] [2]. Both the one-step and Li's combustion mechanisms provides accurate waves-speed estimates, deviating respectively by 1% and 4% from the experimental measurements. Further deviations in plenum pressures are observed, with both mechanisms underpredicting the pressure in the air-plenum and over-predicting the pressure in the fuel plenum. Finally, the largest discrepancies are observed inside the annulus, where the two reaction mechanisms under-predict the pressure by 18% and 25%, respectively. This may be from the sampling only being at the instantaneous measurement at the end of the solution instead of the time average pressure over a few cycles. This remaining difference may be explained by an insufficient spatial resolution, and new simulations using adaptive mesh refinement will be undertaken to verify this hypothesis. Another comparison is the runtimes between the RDE cases, which was not quantified. With the one-step hydrogen case, a solution was attained in 15 cycles (11160 time-steps) with 160 cores in under 12 hours wall clock time. This was substantially faster than the Li Mechanism case which took 5.25 days on same. Future work will investigate settings and solver improvements to the solution time of the Li Mechanism case.

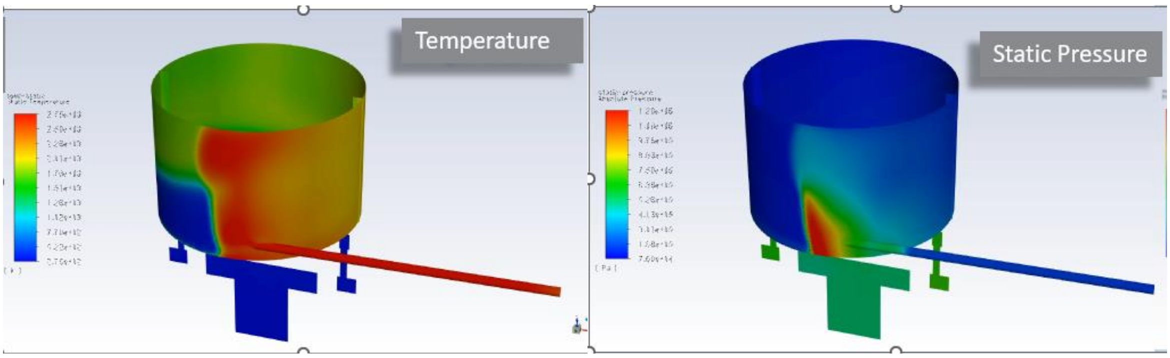

Figure 15: The developed detonation wave shown in the combustor (a) static temperature and (b) static pressure contours for the performance 1-step reacting case.

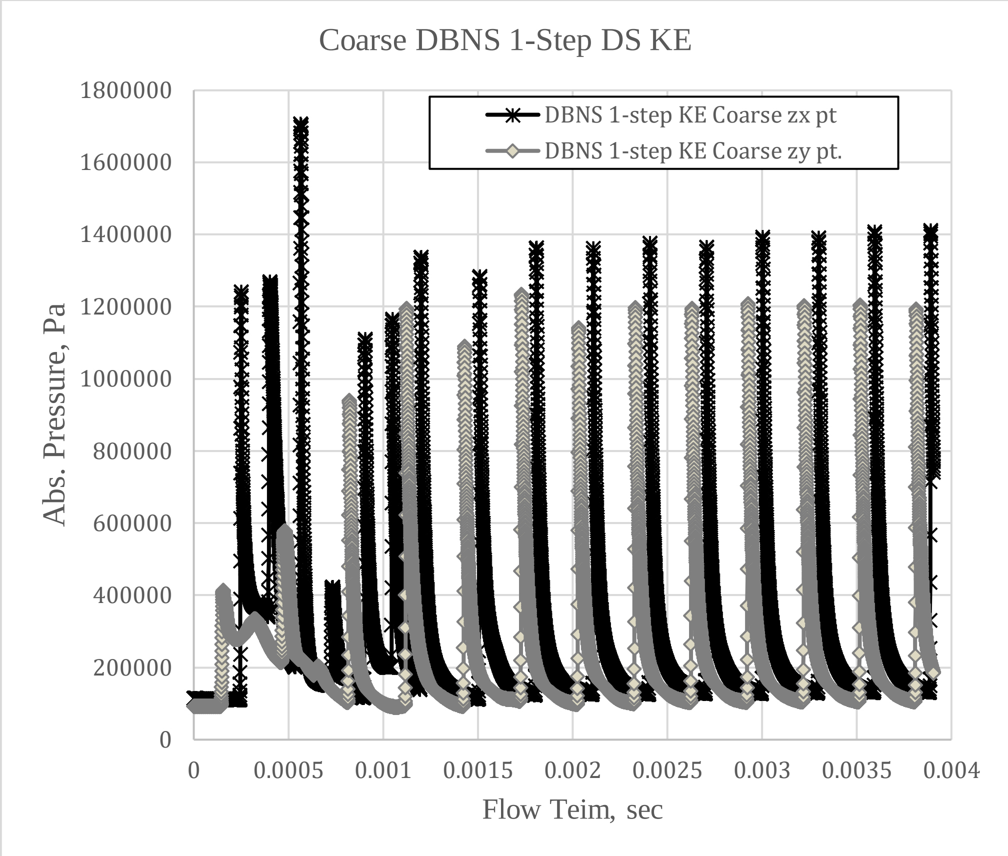

Figure 16: Transient pressure traces Coase DBNS 1-step case in the combustion chamber for the for 11160 timesteps, showing a periodic steady solution start at 0.0018 secs.

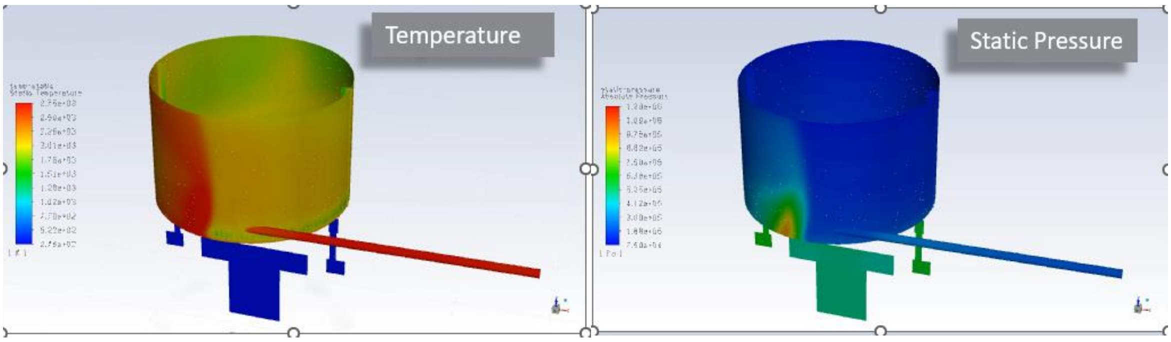

Figure 17: The developed detonation wave shown in the combustor (a) static temperature and (b) static pressure contours for the chemistry case, where the wave is going opposite direction for the Base Li model .

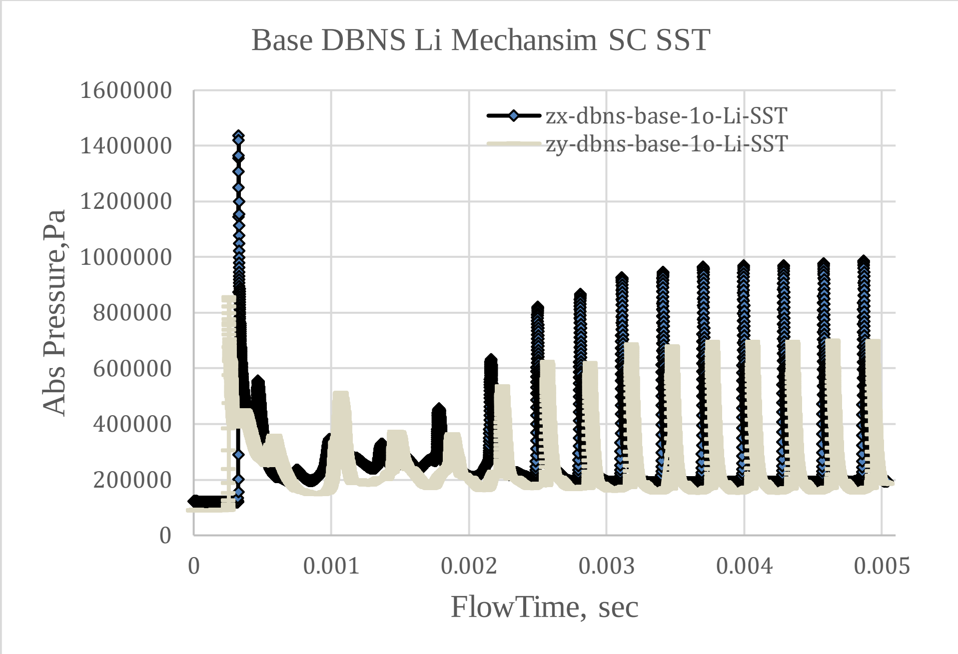

Figure 18: Transient pressure traces in the combustion chamber for the for 11160 timesteps, showing a periodic steady solution start at 0.0025 secs.

Operating Point 0/.63 kg/s	Wave Freq (kHz)	Wave Speed (m/s)	Wave Speed (%CJ)	Air Plenum Pressure (kPa)	Fuel Plenum Pressure (kPa)	Annulus Pressure @2.54 cm (kPa)
(Expt.)	3.78	1740	88.05%	431	503	213
Case 1	3.64	1759	89.01%	410	541	174
delta %	*-3.80%*	*1.10%*	*1.1 0%*	*-4.90%*	*7.60%*	*-18.40%*
Case 2	3.77	1823	92.25%	400	514	158
delta %	*-0.30%*	*4.80%*	*4.80%*	*-7.20%*	*2.30%*	*-25.80%*
Starkey P. et al	3.64	1758	88.96%	470	562	193
delta %	*-3.70%*	*1.00%*	*1.00%*	*9.00%*	*11.70%*	*-9.40%*

Table 2: Comparison of numerical and experimental [1][2] results for each of the cases, reduction of frequencies and other RDE outputs

5 Conclusion and Future Work

The goal of this effort was to validate the Ansys Fluent DBNS solver's new and updated reacting model capabilities against three high-speed combustion experiment results. The three cases represented two different supersonic combustors that are being developed for new turbojet and hypersonic propulsion engines applications. Two of the cases represents scramjet combustors (Burrow-Kurkow supersonic combustor at Mach 2.44, and DLR strut combustor at Mach 2.0) and the third a rotating detonation engine (AFRL/NETL RDE), all operating on hydrogen fuel and air in scaled experimental tests. The comparison between the experiments and the numerically predicted solutions were shown to be in good agreement; noted discrepancies were discussed for each case. From the results of this study, we can make the following conclusions. i) Current development on the

Ansys Fluent DBNS CFD code has made the solver capable of accurately simulating the complex flow physics in these high-speed combustors. ii) All of the chemistry solvers show the capability of providing reasonable solutions to the complex equilibrium and non-equilibrium high-speed reacting flows, each solver showing the differences in modeling methods. We also conclude the need for a database of reliable high-speed reacting experimental data to help develop and validate improvements on these reacting flow models. All these results form a basis to further studies into this class of reacting flows with more comprehensive physical modeling, more time-average transient solutions to compare to steady-state results, and improvements in the turbulence models to deal with shock-boundary-layer physics, so this is only the beginning of what will be built on with this study.

References

[1] Leslie, J., Marren, D., Hypersonic Test Capabilities Overview, U.S. Air Force T&E Days, February 2009.

[2] Candler, G. V., Subbareddy, P. K., Brock J. M., Advances in Computational Fluid Dynamics Methods for Hypersonic Flows, Journal of Spacecraft and Rockets, Vol 52, Issue 1, 2015.

[3] Bertin, J. J., Periaux, J., Ballmann, J., "Advances in Hypersonics: Modeling Hypersonic Flows", Volume 2, ISBN 0817636641, 1992.

[4] Longo, J.M.A. and Hannemann, K. and Hannemann, V., The Challenge of Modeling High Speed Flows, ISBN 978-3-901608-32-2, 2007.

[5] Sunena S, "Supersonic Combustion Ramjet: An Overview." J Aeronaut Aerospace Eng. 10:273, Sept. 202.

[6] Choubey G, Pandey KM. Investigation on the effects of operating variables on the performance of two-strut scramjet combustor. Int J Hydrogen Energy 2016;41(45):20753e70.

[7] Burrows, M. C. and Kurkov, A. P., "Analytical and Experimental Study of Supersonic Combustion of Hydrogen in a Vitiated Airstream," NASA-TM-X-2828, September 1973.

[8] Engblom, W. A., Frate, F. C., and Nelson C. C., "Progress in Validation of Wind-US for Ramjet/Scramjet Combustion," AIAA-2005-1000, January 2005.

[9] Vyas, M. A., Engblom, W. A., Georgiadis, N. J., Trefny, C. J., and Bhagwandin, V. A., "Numerical Simulations of Vitiation Effects on a Hydrogen-fueled Dual-mode Scramjet," AIAA-2010-1127, January 2010.

[10] W. Waidmann, F.Alff, U. Brumund, M. Bohn, W. Clauss, M. Oschwald. Experimental Investigation of the Combustion Process in a Supersonic Combustion Ramjet (SCRAMJET). Deutsher Luft-und Raumfahrtkongres, DGLR-Jahrestagung 1994 Erlangen, 4-7 Oct 1994

[11] MC Burrows and AP Kurkov. An analytical and experimental study of supersonic combustion of hydrogen in vitiated air stream. AIAA Journal, 11(9):1217–1218,1973.

[12] A, Sankaran, K Sundararaj, M Moses Devaprasanna, and N Maheswaran. A CFD Based Numerical Analysis of Scramjet. Int. J. of Eng. Research & Tech., ISSN:2278-0181 Vol 5 Issue 12, 2016

[13] K.M.Pandey, T.Sivasakthivel. CFD Analysis of a Hydrogen Fueled Mixture in ScramjetCombustor with a Strut Injector by Using Fluent Software. IACSIT Inter. J. of Eng. and Tech, Vol.3, No.2, 2011

[14] Z. Xiang, S. Yang, S. Xie, Ji Li, and H. Ren. Turbulence–chemistry interaction models with finite-rate chemistry and compressibility correction for simulation of supersonic turbulent combustion. Eng. App. of Comp. Fluid Mechanics 2020, Vol. 14, No. 1, 1546–1561

[15] C. Gong, M. Jangi, X. Bai, J. Liang, and M. Sun. Large eddy simulation of hydrogen combustion in supersonic flows using an Eulerian stochastic fields method. Inter. J. of Hydrogen Energy 42, 2017 1264-1275

[16] G. Santhanam, C. Srinivas, CH. Khyathi Sree, and S. Srinivas Prasad. CFD Analysis of the Effect of Mach Number on SCRAMjet Combustion. Inte. J. of Mech. and Prod. Eng. Res. and Dev. (IJMPERD) ISSN (P): 2249-6890; ISSN (E): 2249-8001 Vol. 9, Issue 4, 2019, 393-402

[17] M. Berglund, E. Fedina, C. Fureby, J. Tegnér, and V. Sabel'nikov. Finite Rate Chemistry

Large-Eddy Simulation of Self-Ignition in a Supersonic Combustion Ramjet. AIAA J. Vol. 48, No. 3, March 2010

[18] Juan Li, Zhenwei Zhao, Andrei Kazakov, Frederick L. Dryer. An updated comprehensive kinetic model of hydrogen combustion. International Journal of Chemical Kinetics 2004, 36 (10) , 566-575. https://doi.org/10.1002/kin.20026

[19] M. Ferrarotti, Z. Li, A. Parente. On the role of mixing models in the simulation of MILD combustion using finite-rate chemistry combustion models. Proceedings of the Combustion Institute, September 28, 2018

[20] B. A. Rankin, M. L. Fotia, D. E. Paxson, J. L. Hoke, and F.R. Schauer. Experimental and Numerical Evaluation of Pressure Gain Combustion in a Rotating Detonation Engine. AIAA SciTech 5-9 Jan 2015, 53rd AIAA Aero. Sci. Meeting

[21] P. A. Strakey, D. H. Ferguson, A. T. Sisler and A. C. Nix. Computationally Quantifying Loss Mechanisms in a Rotating Detonation Engine. AIAA

[22] J. Sun, J. Zhou, S. Liu, Z. Lin. Numerical investigation of a rotating detonation engine under premixed/non-premixed conditions. Acta Astronautica 152 (2018) 630–638

[23] P. Pal, G. Kumar, S. Drennan, B. Rankin, S. Som. Numerical Modeling of Supersonic Combustion in a Non-Premixed Rotating Detonation Engine. 11th US National Combustion meeting, West.States Sec. of the Combustion Ins., March 24-27, 2019.

[24] ANSYS, Inc., ANSYS Fluent User's Guide, Release 2022R1, 2020.

[25] ANSYS, Inc., ANSYS Fluent Theory, Release 2022R1, 2020.

[26] Kim, S.E., Mathur, S., Murthy, J., Choudhury, D., A Reynolds-averaged Navier-Stokes solver using unstructured mesh-based finite-volume scheme, 36th AIAA Aerospace Sciences Meeting and Exhibit, 1998.

[27] Kim, S.E., Makarov, B., An implicit fractional-step method for efficient transient simulation of incompressible flows, 17th AIAA Computational Fluid Dynamics Conference, 2005.

[28] Weiss, J. W., Maruszewski, J. P., Smith, W. A., Implicit Solution of Preconditioned Navier-Stokes Equations Using Algebraic Multigrid, AIAA Journal, Volume 37, Number 1, January 1999.

[29] Weiss, J. W., Smith, W. A., Preconditioning Applied to Variable and Constant Density Flows, AIAA Journal, Volume 33, Number 11, January 1995.

[30] Barth, T. J., Jespersen, D., The design and application of upwind schemes on unstructured meshes, AIAA-89-0366. AIAA 27th Aerospace Sciences Meeting, Reno, Nevada. 1989.